

Research Paper

The human somatostatin receptor type 2 as an imaging and suicide reporter gene for pluripotent stem cell-derived therapy of myocardial infarction

Katrien Neyrinck^{1,2*}, Natacha Breuls^{3*}, Bryan Holvoet^{1*}, Wouter Oosterlinck⁴, Esther Wolfs⁵, Hubert Vanbilloen¹, Olivier Gheysens¹, Robin Duelen³, Willy Gsell⁶, Ivo Lambrichts⁵, Uwe Himmelreich⁶, Catherine M. Verfaillie², Maurilio Sampaolesi³, Christophe M. Deroose¹✉

1. Nuclear Medicine and Molecular Imaging, Department of Imaging and Pathology, KU Leuven, Belgium.
2. Stem Cell Institute Leuven, Department of development and regeneration, KU Leuven, Belgium.
3. Translational Cardiology Lab, Department of Development and Regeneration, KU Leuven, Belgium.
4. Cardiac Surgery, Department of Cardiovascular Sciences, KU Leuven, Belgium.
5. Lab of Histology, Department of Morphology, Biomedical Research Institute, Universiteit Hasselt, Belgium.
6. Biomedical MRI Unit, Department of Imaging and Pathology, KU Leuven, Belgium.

* Equal contribution to this work

✉ Corresponding author: Prof. Dr. Christophe Deroose, UZ Leuven, Division of Nuclear Medicine, Campus Gasthuisberg, Herestraat 49, B-3000 Leuven. Tel: +32 16 34 37 12; Fax: +32 16 34 37 59; christophe.deroose@uzleuven.be

© Ivyspring International Publisher. This is an open access article distributed under the terms of the Creative Commons Attribution (CC BY-NC) license (<https://creativecommons.org/licenses/by-nc/4.0/>). See <http://ivyspring.com/terms> for full terms and conditions.

Received: 2017.09.25; Accepted: 2018.02.28; Published: 2018.04.14

Abstract

Rationale: Pluripotent stem cells (PSCs) are being investigated as a cell source for regenerative medicine since they provide an infinite pool of cells that are able to differentiate towards every cell type of the body. One possible therapeutic application involves the use of these cells to treat myocardial infarction (MI), a condition where billions of cardiomyocytes (CMs) are lost. Although several protocols have been developed to differentiate PSCs towards CMs, none of these provide a completely pure population, thereby still posing a risk for neoplastic teratoma formation. Therefore, we developed a strategy to (i) monitor cell behavior noninvasively via site-specific integration of firefly luciferase (Fluc) and the human positron emission tomography (PET) imaging reporter genes, sodium iodide symporter (hNIS) and somatostatin receptor type 2 (hSSTR2), and (ii) perform hSSTR2-mediated suicide gene therapy via the clinically used radiopharmaceutical ¹⁷⁷Lu-DOTATATE.

Methods: Human embryonic stem cells (ESCs) were gene-edited via zinc finger nucleases to express Fluc and either hNIS or hSSTR2 in the safe harbor locus, adeno-associated virus integration site 1. Firstly, these cells were exposed to 4.8 MBq ¹⁷⁷Lu-DOTATATE *in vitro* and cell survival was monitored via bioluminescence imaging (BLI). Afterwards, hNIS⁺ and hSSTR2⁺ ESCs were transplanted subcutaneously and teratomas were allowed to form. At day 59, baseline ¹²⁴I and ⁶⁸Ga-DOTATATE PET and BLI scans were performed. The day after, animals received either saline or 55 MBq ¹⁷⁷Lu-DOTATATE. Weekly BLI scans were performed, accompanied by ¹²⁴I and ⁶⁸Ga-DOTATATE PET scans at days 87 and 88, respectively. Finally, hSSTR2⁺ ESCs were differentiated towards CMs and transplanted intramyocardially in the border zone of an infarct that was induced by left anterior descending coronary artery ligation. After transplantation, the animals were monitored via BLI and PET, while global cardiac function was evaluated using cardiac magnetic resonance imaging.

Results: Teratoma growth of both hNIS⁺ and hSSTR2⁺ ESCs could be followed noninvasively over time by both PET and BLI. After ¹⁷⁷Lu-DOTATATE administration, successful cell killing of the hSSTR2⁺ ESCs was achieved both *in vitro* and *in vivo*, indicated by reductions in total tracer lesion uptake, BLI signal and teratoma volume. As undifferentiated hSSTR2⁺ ESCs are not therapeutically relevant, they were differentiated towards CMs and injected in immune-deficient mice with a MI. Long-term cell survival could be monitored without uncontrolled cell proliferation. However, no improvement in the left ventricular ejection fraction was observed.

Conclusion: We developed isogenic hSSTr2-expressing ESCs that allow noninvasive cell monitoring in the context of PSC-derived regenerative therapy. Furthermore, we are the first to use the hSSTr2 not only as an imaging reporter gene, but also as a suicide mechanism for radionuclide therapy in the setting of PSC-derived cell treatment.

Key words: noninvasive imaging; stem cell therapy; myocardial infarction; suicide gene

Introduction

Myocardial infarction (MI) is one of the major reasons for mortality in the western world. It is caused by a temporary or permanent occlusion of one of the coronary arteries, resulting in an ischemic area and the loss of billions of cardiomyocytes (CMs). As CMs have only a limited proliferative capacity (annual turnover rate of less than 1%), the heart is unable to recover from this massive cell loss. Therefore, stem cells and more specifically pluripotent stem cell (PSC)-derived CMs have been investigated for their potential to repopulate the damaged heart [1-5].

PSCs have an indefinite self-renewal capacity and are able to differentiate towards every cell type of the human body. Hence, they have an enormous potential within regenerative medicine. Unfortunately, differentiation protocols do not provide a pure CM population, thereby potentially leaving undifferentiated cells that can form a teratoma, a neoplastic lesion containing cells of the three germ layers [6]. Despite this risk, numerous pre-clinical studies have demonstrated that PSC-derived CMs are able to couple with the host myocardium and partially repair a MI [1-4]. Moreover, a patient suffering from a MI showed improvements after receiving an injection with PSC-derived cardiovascular progenitors. However, no direct link between the cell injection and the observed improvement could be drawn as the patient also received a coronary bypass [7].

Currently, tissue sampling is the golden standard to follow-up cell engraftment in the clinic, thereby limiting information on the behavior, localization and viability of the cells over time. Therefore, imaging methods have been developed to noninvasively monitor stem cell distribution [8, 9]. Here, we have focused on reporter gene imaging as it allows long-term cell tracking and only visualizes viable cells [8].

Previously, exogenous genes were incorporated randomly in the genome using viral vectors. This can potentially induce insertional mutagenesis and unstable reporter gene expression [10]. Furthermore, a heterogeneous cell population will be generated, as cells will bear different copy numbers of the reporter gene [11, 12]. Therefore, alternative gene-editing

strategies have been developed for site-specific reporter gene integration. One example is the use of zinc finger nucleases (ZFNs), consisting of a DNA binding domain, a zinc finger, and an endonuclease domain, FokI. Upon dimerization, a double strand DNA break is generated that can be repaired either by non-homologous end joining or by homologous recombination if a donor plasmid is provided with homologous sequences towards the regions of the double stranded DNA breaks [13]. The adeno-associated virus integration site 1 (AAVS1) locus, encoding the ubiquitously expressed protein phosphatase 1 regulatory subunit 12 C on chromosome 19, is a known 'safe harbor' locus, meaning that integration of foreign material does not evoke pathological responses and perturbs neither proliferation nor the characteristics of the cell. In addition, this region is always located in open chromatin and is not hampered with reporter gene silencing [13, 14]. These features make targeted integration into the AAVS1 locus a better and safer strategy to express exogenous genes.

The radionuclide imaging reporter genes human somatostatin receptor type 2 (hSSTr2) and human sodium iodide symporter (hNIS) were chosen as they both are of human origin and allow cell tracking using clinical radionuclide imaging devices. Different groups have already demonstrated the ability to monitor stem cells in the heart via the hNIS [15-17], but this has not been demonstrated for hSSTr2. Furthermore, therapeutic radiopharmaceuticals, such as ¹⁷⁷Lu-DOTATATE, have been shown to specifically target hSSTr2-overexpressing tumors, resulting in prolonged progression-free survival in patients with midgut neuroendocrine tumors (NETs) [18].

In this study, we explored the possibility to gene-edit and monitor human embryonic stem cells (ESCs) by both radionuclide imaging reporter genes (hSSTr2 and hNIS). Furthermore, we assessed if hSSTr2 could be used as a suicide gene in case of uncontrolled cell proliferation. After differentiation towards CMs, we assessed the feasibility of long-term cell tracking via bioluminescence imaging (BLI) and small animal positron emission tomography (PET) and the potential therapeutic efficacy using cardiac magnetic resonance imaging (MRI).

Materials

Cell culture

H9 (WA09, WiCell Research Institute, Madison, USA) human ESCs were cultured and gene-edited as described previously [19].

Cardiac differentiation

According to the PSC CM Differentiation Kit (Gibco, Waltham, MA, USA), ESCs were differentiated towards CMs.

Gene expression analysis

RNA was isolated using the PureLink RNA Mini Kit (Invitrogen, Carlsbad, CA, USA) and 500 ng of RNA was retro-transcribed into cDNA using the Superscript III Reverse Transcriptase First-Strand Synthesis SuperMix (Invitrogen). Next, quantitative real-time PCR (qRT-PCR) was performed with the Platinum SYBR Green qRT-PCR SuperMix-UDG (Invitrogen). The cycle consisted of 2 min at 95 °C followed by 40 cycles of 15 s at 95 °C and 45 s at 60 °C. All primers are listed in **Table 1**.

Table 1. Primers for qPCR

	Primer	Primer Sequence
Pluripotency markers (human)		
OCT4	Forward	CGAGCAATTGCCAAGCTCCTGAA
	Reverse	GCCGCAGCTTACACATGTTCTTGA
SOX2	Forward	TGGCGAACCATCTCTGTGGT
	Reverse	CCAACGGTGTCAACCTGCAT
NANOG	Forward	GATTTGTTGGCCCTGAAGAAA
	Reverse	AAGTGGTGTGTTTGCCTTTG
C-MYC	Forward	TCCTCGGATTCCTCTGCTCTCT
	Reverse	AGAAGGTGATCCAGACTCTGACCT
Cardiac markers (human)		
TBX5	Forward	CTGTGGCTAAAATCCACGAAGT
	Reverse	GTGATCGTCGGCAGGTACAAT
cMHC	Forward	GCCCTTGACATTCGCACTG
	Reverse	CGGGACAAAATCTTGGCTTTGA
Housekeeping genes (human)		
RPL13a	Forward	CCTGGAGGAGAAGAGGAAAGAGA
	Reverse	TTGAGGACCTCTGTGATTTGTCAA
TMEM85	Forward	CGCTTCAAGTGGGCCATTTG
	Reverse	ACTGGGTAGAGCGAGTCTCC
GLUSB	Forward	GTCTGCGGCATTTGTTCGG
	Reverse	CACACGATGGCATAGGAATGG

Immunofluorescence

ESC-derived CMs were fixed and stained according to the protocol previously described [20] with rabbit anti-CX-43 (1/1000, Abcam, Cambridge, United Kingdom) primary antibody at 4 °C, overnight. Next, the cells were stained with anti-rabbit Alexa fluorophore 488 (1/500, Invitrogen, Thermo Fisher Scientific) and mouse anti- α -smooth muscle actin (α SMA)-Cy3 antibody at room temperature for 60 min and 2 h, respectively. Afterwards, Hoechst (1/1000, Sigma-aldrich, Saint

Louis, Missouri, USA) staining was performed for 5 minutes.

Teratoma assay

The Ethical Committee of the KU Leuven (P160/2015 & P096/2016) approved all animal experiments. Five-week-old female thymic aplasia nude (NMRI-nu; Janvier Labs) mice (~20 g) were subcutaneously injected with 1.5-2 million ESCs expressing either hNIS (injection right side) or hSSTR2 (injection left side) (n=17). During this procedure, the mice were anaesthetized with 3% isoflurane (IsoVET, 100 mg/g, Eurovet, Piramal Healthcare) in 100% O₂ (flow rate 2 L/min).

Bioluminescence imaging

In vitro BLI experiments were performed as described previously [19]. Briefly, cells were incubated with 0.3 mg/L D-luciferin (Promega, Benelux, Leiden, The Netherlands) and light photons were detected with the IVIS Spectrum (Caliper Life Sciences, Hopkington, MA, USA).

For the *in vivo* BLI, mice were sedated with 2-3% isoflurane in 100% O₂ (2 L/min) and subcutaneously injected with 126 mg/kg D-luciferin (Promega). Light photons were detected with the IVIS Spectrum (Caliper Life Sciences).

Radionuclide experiments

Tracer uptake

Tracer uptake experiments were performed as previously described [19].

Efflux of ^{99m}TcO₄⁻ and ⁶⁸Ga-DOTATATE from hNIS⁺ and hSSTR2⁺ cells was measured by incubating the cells with ^{99m}TcO₄⁻ and ⁶⁸Ga-DOTATATE, respectively for 1 h or 10 min, followed by an incubation with tracer-free DMEM for 5, 15, 30 and 60 min. Afterwards, the same steps were used as previously described [19].

¹⁷⁷Lu-DOTATATE treatment

In vitro: hNIS⁺ or hSSTR2⁺ ESCs were plated on matrigel-coated 24-well plates and kept under normoxic conditions. The following day, a baseline *in vitro* BLI scan was performed. Next, hSSTR2⁺ ESCs and hNIS⁺ ESCs were exposed to either PBS (vehicle) or 4.8 MBq ¹⁷⁷Lu-DOTATATE for 1 h followed with 5 times of rinsing. Follow-up BLI scans were performed 2, 4 and 6 days after exposure.

In vivo: The animals with subcutaneous teratomas received an intravenous tail injection of 55.5 MBq of ¹⁷⁷Lu-DOTATATE or sterile saline, 60 days after cell injection.

Small animal PET

hSSTR2⁺ and hNIS⁺ ESCs were visualized by an intravenous injection of 5-7 MBq ⁶⁸Ga-DOTATATE or ¹²⁴I, respectively. A 20 min static scan was acquired 2 h after ¹²⁴I and 1 h after ⁶⁸Ga-DOTATATE administration, using the Focus 220 small-animal PET system (Siemens Medical Solutions, Knoxville, TN, USA). For every scan, a transmission scan was obtained using a ⁵⁷Co-source (5 mCi; Eckert & Ziegler, Berlin, Germany). During injection and PET imaging, mice were anaesthetized with 2-3% isoflurane (Piramal Healthcare) in 100% O₂ (2 L/min). PET images were reconstructed through a maximum a posteriori (MAP) reconstruction algorithm and further analyzed with PMOD 3.0 (PMOD technologies, Zürich, Switzerland). Images were converted to standardized uptake values (SUV), calculated according to the following formula:

$$\text{SUV} = \frac{\text{activity concentration in organ}}{\text{activity / weight of the animal}}$$

Volumes of interest (VOI) were positioned manually around the graft regions with the contralateral side as control.

Intra-myocardial cell injection and myocardial infarct model

For intra-myocardial cell (n=4) or sham (n=4) injection, 12-week-old Rag2/γc^{-/-} mice (body weight ≥22 g) were anaesthetized via intraperitoneal injection of 5 mg/mL ketamine (Nimatek, 100 mg/mL, Eurovet, Piramal Healthcare) and 0.05 mg/mL domitor (1 mg/mL, Vétoquinol, Lure cedex, France) and subsequently 0.05 mg/mL atropine (0.5 mg/mL, Sterop Group, Brussels, Belgium). Mechanical ventilation (Minivent 845; Hugo Sachs/Harvard Apparatus, March-Hugstetten, Germany) was started with 50% oxygenated air, a tidal volume of three times body weight + 155 μL and respiratory rate of 135 strokes/min. First, a MI was generated by permanent occlusion of the left anterior descending coronary artery (LAD), as previously described [21]. Afterwards, the mice received three injections of either CMs, each time 1 million hSSTR2⁺ ESC-derived CMs, or sham injections in the border region of the infarct. Afterwards, the mice were awakened by intraperitoneal administration of 0.25 mg/mL Antisedan (5.0 mg/mL, Vétoquinol). During the surgical procedure, ECG was monitored and the body temperature was maintained at physiological levels of 37±1 °C.

Cardiac MRI

MRI measurements were performed 3-5 days before inducing a MI. Immediately after the induction

of a MI, cells or matrigel (sham) were injected and MRI scans were obtained 1, 2 and 4 weeks after MI induction. Mice were anaesthetized with isoflurane (induction: 2-3%, during measurement: 1.5-2%, both in O₂) and adjusted to keep respiration rate at 100-120 breaths per minute. Body temperature was maintained at 37±1 °C. Cardiac MRI was performed using a small animal MRI scanner (Bruker Biospec 70/30; field strength 7 T; horizontal bore 30 cm; Bruker BioSpin, Ettlingen, Germany) equipped with an actively shielded gradient insert (200 mT/m) and quadrature volume coil (Bruker Biospin). MRI protocols were similar to previously described experiments [21]. Briefly, after planning the geometry of the short axis view of the heart, two-dimensional short- and long-axis T1-weighted bright blood images were recorded using FLASH self-gated sequences (intragate) (repetition time = 10.32 ms; echo time = 3.92 ms; flip angle = 20°, field-of-view = 25 mm × 25 mm; matrix = 128×128; slice thickness = 1 mm throughout the heart). For image processing, the software Paravision 6 (Bruker Biospin) was used. Afterwards, left ventricular ejection fraction (LVEF) were manually calculated using the formula described below:

$$\text{EF} = \frac{(\text{end diastolic volume} - \text{end systolic volume})}{\text{end diastolic volume}}$$

Statistical analysis

Data are presented as mean ± SD. One-way or two-way ANOVA was performed with a Tukey post-hoc test if the samples were normally distributed and had equal variances. Otherwise, the Kruskal-Wallis test was performed followed by the Dunns post-hoc test. P-values < 0.05 were considered statistically significant. Data were processed using GraphPad Prism version 5.00 for Windows (GraphPad Software, San Diego, California, USA).

Results

Embryonic stem cells maintained pluripotency and had functional reporter gene expression after gene-editing via zinc finger nucleases

Two human ESC lines expressing two different radionuclide reporter genes (hSSTR2⁺ and hNIS⁺ ESCs) were generated through ZFN-mediated site-specific integration in the AAVS1 locus. Besides the radionuclide reporter genes, eGFP and firefly luciferase (Fluc) were present in the cassette. The reporter gene cassette was driven by the hybrid CAGGS promoter. qPCR analysis showed similar expression values of pluripotency transcription factors OCT4, NANOG, SOX2 and C-MYC before and after gene-editing (Figure 1A).

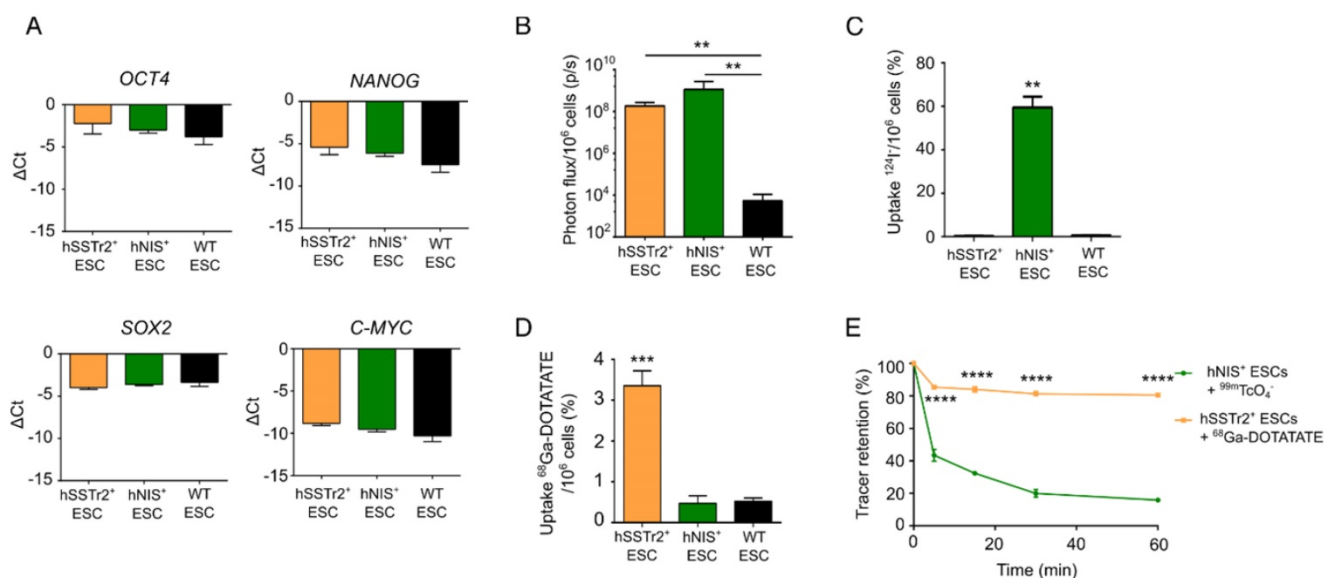


Figure 1. *In vitro* validation of pluripotency and imaging reporter gene expression in gene-edited hESC. **(A)** qRT-PCR analysis showed that expression of pluripotency markers *OCT4*, *SOX2*, *NANOG* and *C-MYC* was not significantly different between hSSTR2⁺, hNIS⁺ and WT ESCs. **(B)** Quantitative analysis showed a high BLI signal in both gene-edited ESCs, which was significantly different compared to WT ESCs (**; $p < 0.01$) ($n = 3$ independent experiments (IEs)). **(C)** Uptake experiments with ¹²⁴I- showed specific tracer uptake in hNIS⁺ ESCs (**; $p < 0.0001$) ($n = 3$ technical replicates (TRs)). **(D)** Uptake experiments with ⁶⁸Ga-DOTATATE showed specific tracer uptake in hSSTR2⁺ ESCs (**; $p < 0.001$) ($n = 3$ IEs). **(E)** After removal of tracer-containing medium with non-radioactive medium, a rapid efflux of ^{99m}TcO₄ from hNIS⁺ cells could be observed. However, ~15% of the tracer remained inside the cell after one hour. In contrast, stable ⁶⁸Ga-DOTATATE retention was shown in hSSTR2⁺ ESCs with ~80% of the tracer maintained inside the cell after one hour.

Gene-edited ESCs showed a functional Fluc expression as they produced BLI signals after incubation with D-luciferin, while only background values were obtained in wild-type (WT) ESCs (fold change: $>10^5$; $p < 0.01$; **Figure 1B**). The functionality of both radionuclide reporter genes was assessed by *in vitro* radioligand uptake experiments. Cells were incubated with ¹²⁴I and after one hour, $59.5 \pm 8.6\%$ of ¹²⁴I was taken up by hNIS⁺ ESCs. This uptake was ~100 times higher compared to hSSTR2⁺ and WT ESCs ($p < 0.001$; **Figure 1C**). hSSTR2⁺ ESCs were able to bind $3.4 \pm 0.4\%$ of ⁶⁸Ga-DOTATATE after one hour of incubation and thus showed ~7 times more tracer binding than hNIS⁺ and WT ESCs ($p < 0.001$; **Figure 1D**). To evaluate tracer retention, hNIS⁺ ESCs and hSSTR2⁺ ESCs were incubated for one hour with ^{99m}TcO₄ and ⁶⁸Ga-DOTATATE, respectively, followed by re-incubation with cold medium for various periods of time. A rapid reduction in tracer retention was observed in hNIS⁺ ESCs with only ~15% of the tracer remaining intracellular after one hour. In contrast, stable ⁶⁸Ga-DOTATATE retention was shown in hSSTR2⁺ ESCs ($80.5 \pm 0.8\%$ after one hour; **Figure 1E**). In general, the tracer retention in hSSTR2⁺ ESCs was significantly higher compared to the tracer retention in hNIS⁺ ESCs for all evaluated time points ($p < 0.0001$).

Selective killing of hSSTR2-expressing embryonic stem cells by ¹⁷⁷Lu-DOTATATE

To evaluate if ¹⁷⁷Lu-DOTATATE specifically

targets hSSTR2-expressing cells, both hNIS⁺ and hSSTR2⁺ ESCs were exposed to 4.8 MBq of the radiopharmaceutical. Afterwards, cell viability was assessed by *in vitro* BLI. Results were plotted as relative BLI signals, the photon flux of each condition at each time point divided by the photon flux before exposure (**Figure 2**). Both hNIS⁺ and hSSTR2⁺ ESCs showed an increase in BLI signal over time when not treated with ¹⁷⁷Lu-DOTATATE (hNIS⁺ day 2: 2.0 ± 1.1 and day 6: 9.9 ± 1.3 ; hSSTR2⁺ day 2: 1.2 ± 0.1 and day 6: 8.3 ± 0.5). hNIS⁺ ESCs exposed to ¹⁷⁷Lu-DOTATATE showed a similar increase in BLI signal (day 2: 1.5 ± 0.4 day 6: 8.6 ± 1.0). In contrast, hSSTR2⁺ ESCs exposed to ¹⁷⁷Lu-DOTATATE showed a significantly lower BLI signal than the untreated group at day 4 (0.3 ± 0.2 ; $p < 0.0001$) and day 6 (0.5 ± 0.3 ; $p < 0.0001$). No differences were observed between untreated and ¹⁷⁷Lu-DOTATATE hNIS⁺ ESCs. Afterwards, these findings were confirmed through nuclear staining (**Figure S1**).

To validate the potential of ¹⁷⁷Lu-DOTATATE to specifically kill hSSTR2⁺ ESCs *in vivo*, hSSTR2⁺ and hNIS⁺ teratomas were grown subcutaneously on the left and right flank of nude mice, respectively. At day 59, animals received a baseline small-animal PET scan with ⁶⁸Ga-DOTATATE. Clear focal uptake of ⁶⁸Ga-DOTATATE was observed on the left flank of the animals, where hSSTR2⁺ ESCs were injected, while no specific tracer uptake was present on the contralateral side (**Figure 3A-B**). At day 60 post cell-injection, animals received either 55.5 MBq ¹⁷⁷Lu-DOTATATE

(n=10) or saline (n=7), intravenously. At day 87, another small-animal PET scan with ^{68}Ga -DOTATATE was performed and total lesion uptake was plotted relative to the baseline total lesion uptake. In the animals receiving ^{177}Lu -DOTATATE, a decreased total lesion uptake of $65\pm 7\%$ was observed in the hSSTR2⁺ teratomas compared to baseline. In contrast, hSSTR2⁺ teratomas exposed to saline had an increased total lesion uptake of $67\pm 25\%$ after 28 days (Figure 3C). Therefore, a significant reduction in relative total lesion uptake was observed in hSSTR2⁺ teratomas treated with ^{177}Lu -DOTATATE ($p < 0.0001$).

To evaluate the effect of ^{177}Lu -DOTATATE on hNIS⁺ teratomas, animals were scanned with ^{124}I on day 59 (baseline) and at day 88 (n=4). At day 59, clear focal ^{124}I uptake could be observed on the right flank of the mice, which was not present on the contralateral side (Figure 3D-E). After receiving either ^{177}Lu -DOTATATE or saline at day 60, no significant differences in relative total ^{124}I lesion uptake were demonstrated at day 88 between both groups (saline: $113\pm 23\%$; ^{177}Lu -DOTATATE: $100\pm 18\%$; Figure 3F).

Throughout this experiment, teratoma volumes were macroscopically monitored using a Caliper. Similar baseline teratoma volumes were shown at day 59 for both the saline (hSSTR2⁺: $87\pm 18\text{ mm}^3$; hNIS⁺: $77\pm 16\text{ mm}^3$) and the ^{177}Lu -DOTATATE (hSSTR2⁺: $74\pm 12\text{ mm}^3$; hNIS⁺: $80\pm 16\text{ mm}^3$) exposed groups. Starting from day 73, a significant reduction in teratoma volume could be observed in ^{177}Lu -DOTATATE-treated teratomas expressing hSSTR2

($36\pm 13\text{ mm}^3$) compared to saline-injected hSSTR2⁺ teratomas ($117\pm 14\text{ mm}^3$; $p < 0.05$) (Figure 3G). This reduced teratoma volume remained until the end of the experiment at day 88 (saline: $169\pm 62\text{ mm}^3$; ^{177}Lu -DOTATATE: $28\pm 8\text{ mm}^3$; $p < 0.01$). In contrast, no shrinkage of hNIS⁺ teratomas exposed to ^{177}Lu -DOTATATE (day 88: $110\pm 15\text{ mm}^3$) was observed compared to saline-injected ones (day 88: $100\pm 39\text{ mm}^3$) (Figure 3H).

In the same animals, teratoma kinetics were monitored via BLI (Figure 4A). As before, BLI signals were quantified using the relative changes to baseline. Six days after treatment, a lower relative BLI signal was shown in the hSSTR2⁺ teratomas receiving ^{177}Lu -DOTATATE ($70\pm 13\%$) compared to the saline-treated group ($240\pm 109\%$; $p < 0.05$). This difference remained consistent throughout the rest of the experiment but was only significantly different at day 80 (^{177}Lu -DOTATATE treated group: $47\pm 6\%$; saline-treated group: $190\pm 59\%$; $p < 0.05$) (Figure 4B). For the hNIS⁺ teratomas, no difference in relative BLI signal could be observed between animals receiving either ^{177}Lu -DOTATATE (day 66: $186\pm 26\%$; day 80: $171\pm 76\%$) or saline (day 66: $288\pm 189\%$; day 80: $202\pm 109\%$) (Figure 4C).

Histological examination of hSSTR2⁺ teratomas exposed to ^{177}Lu -DOTATATE showed large vacuoles and deteriorated morphology, while saline-exposed hSSTR2⁺ teratomas remained intact and showed clear cellular structures of the three germ layers (data not shown).

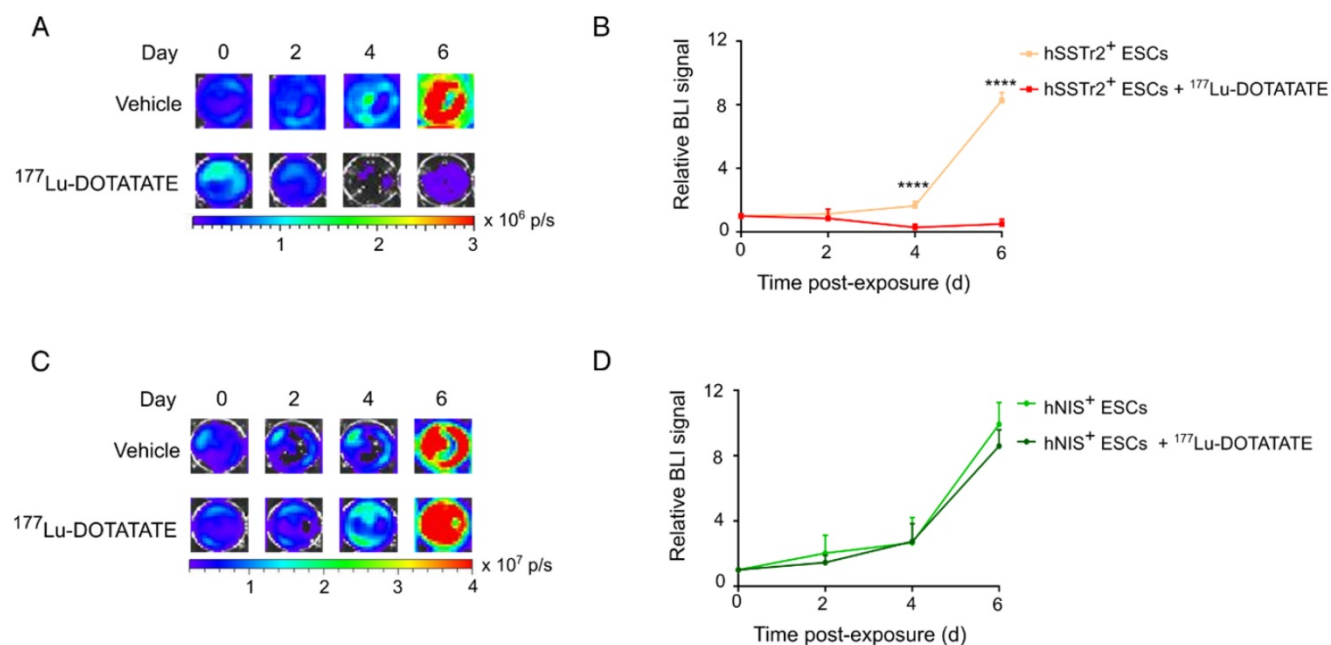


Figure 2. ^{177}Lu -DOTATATE selectively killed hSSTR2⁺ ESCs *in vitro*. (A) hSSTR2⁺ and hNIS⁺ ESCs were exposed for one hour to either 4.8 MBq of ^{177}Lu -DOTATATE or PBS. BLI was performed before and 2, 4 and 6 days after ^{177}Lu -DOTATATE or PBS exposure. Representative BLI images of the hSSTR2⁺ ESCs demonstrated a decrease in BLI signal in ^{177}Lu -DOTATATE-exposed hSSTR2⁺ ESCs over time with a mild recovery at day 6, while an increase in BLI signal was seen in the untreated group. (B) Quantification of the relative BLI signals demonstrated a significant reduction in BLI signal on day 4 and 6 post ^{177}Lu -DOTATATE exposure compared to the untreated group (**** $p < 0.0001$). (C) Representative BLI images of hNIS⁺ ESCs. (D) Quantification of the relative BLI signals showed no difference in cell viability between the ^{177}Lu -DOTATATE- or untreated groups.

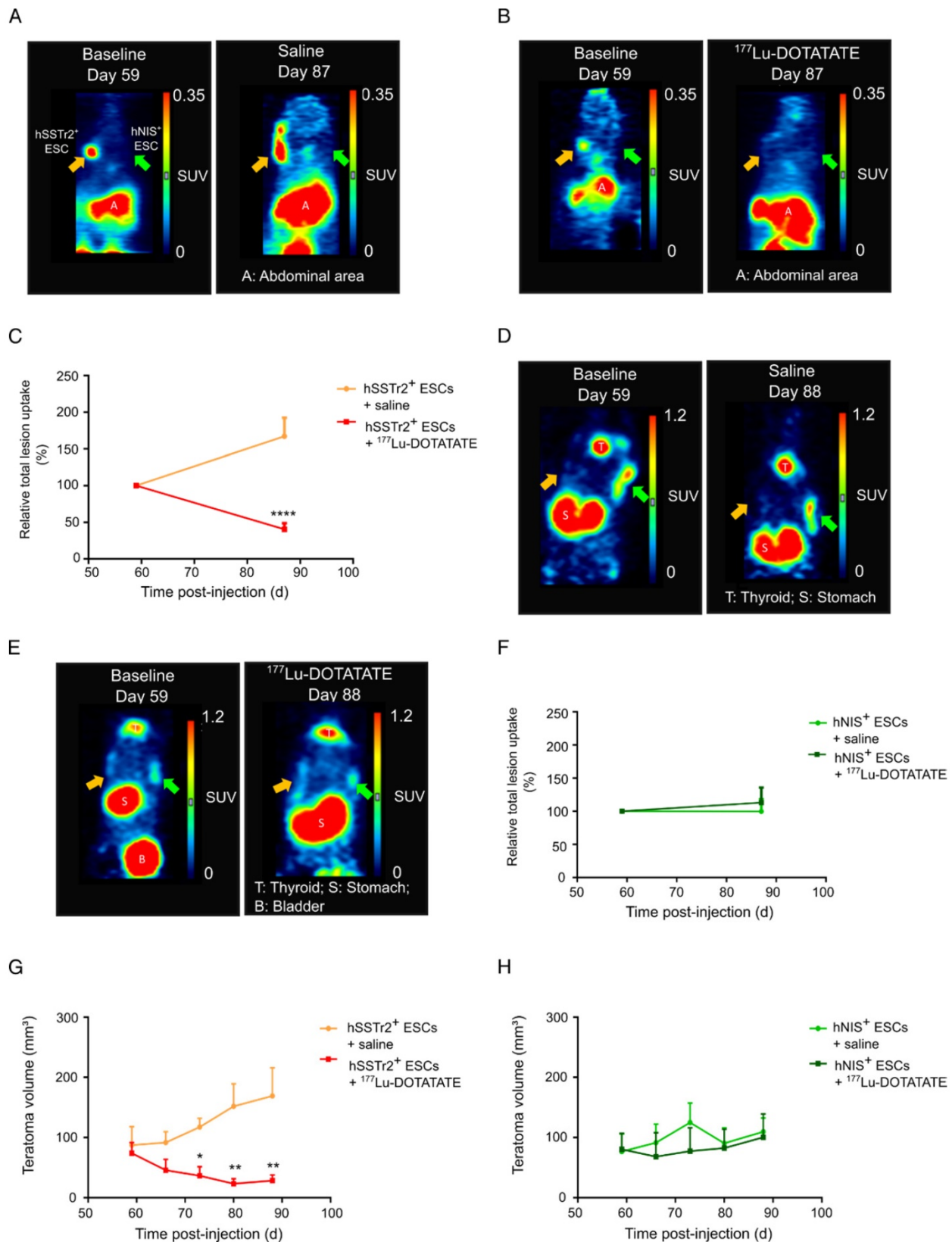


Figure 3. ¹⁷⁷Lu-DOTATATE selectively killed hSSTR2⁺ teratomas as demonstrated by small-animal PET and macroscopic tumor measurements. Representative small-animal PET images after intravenous administration of ⁶⁸Ga-DOTATATE before and 27 days after intravenous saline (A) or ¹⁷⁷Lu-DOTATATE (B) injection. (C) Relative total lesion uptake of hSSTR2⁺ teratomas, i.e., the total lesion uptake of ⁶⁸Ga-DOTATATE divided by the total lesion uptake before saline or ¹⁷⁷Lu-DOTATATE injection, demonstrated a significant decrease in animals injected with ¹⁷⁷Lu-DOTATATE (n=10) compared to saline-injected animals (n=7) (****p<0.0001). Representative small-animal PET images after intravenous administration of ¹²⁴I- before and 28 days after intravenous saline (D) or ¹⁷⁷Lu-DOTATATE (E) injection. (F) Relative total lesion uptake of hNIS⁺ teratomas demonstrated no difference between animals injected with saline (n=4) or with ¹⁷⁷Lu-DOTATATE (n=4). (G) hSSTR2⁺ teratoma volumes significantly decreased upon exposure to ¹⁷⁷Lu-DOTATATE compared to saline-treated groups (*p<0.05; **p<0.01). (H) No difference in teratoma volumes was observed between hNIS-expressing teratomas exposed to either saline or ¹⁷⁷Lu-DOTATATE.

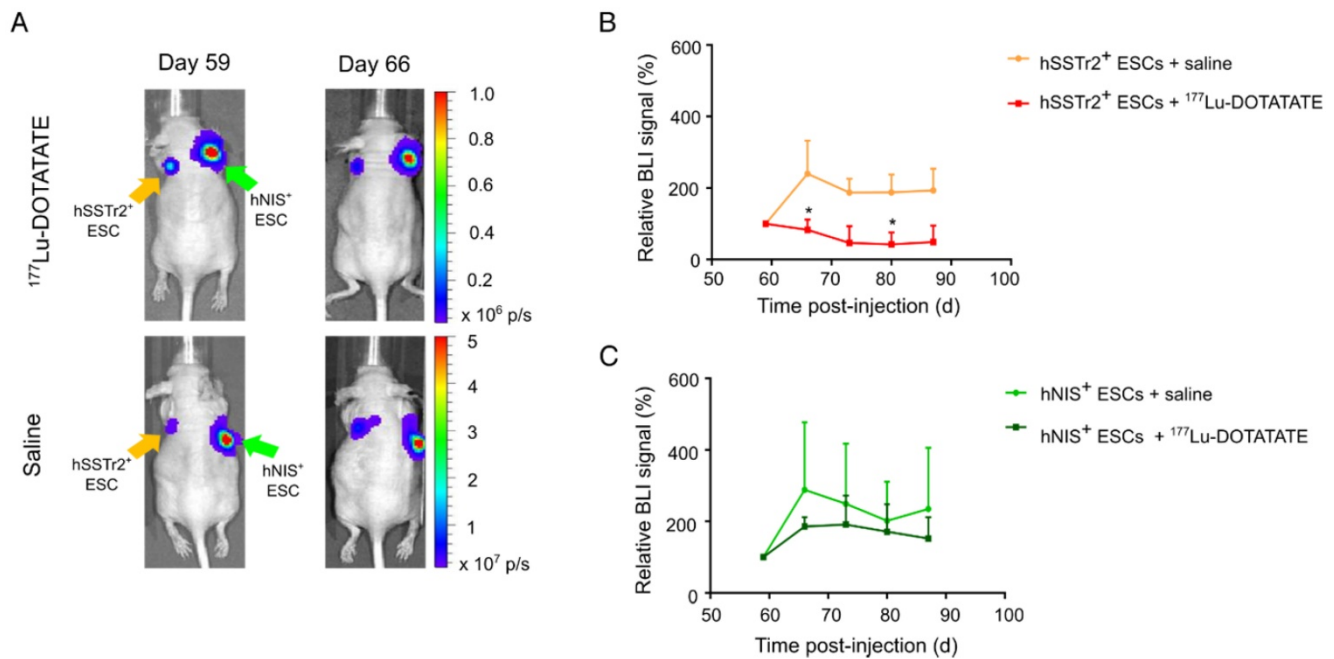


Figure 4. Selective cell killing of $^{177}\text{Lu-DOTATATE}$ as demonstrated by BLI. (A) Representative BLI images of mice receiving either $^{177}\text{Lu-DOTATATE}$ or saline. Day 59 is the day before treatment and day 66 is the first BLI measurement after treatment. A reduction in the BLI signal was seen after 7 days in the hSSTR2⁺ cell graft, while no reduction in BLI signal was present in the hNIS⁺ cell graft. In the saline-treated group, both hSSTR2⁺ and hNIS⁺ teratomas did not show signs of reduced BLI signal. **(B)** Quantification of the relative BLI signals of hSSTR2⁺ teratomas exposed to either $^{177}\text{Lu-DOTATATE}$ (n=10) or saline (n=7) showed a reduction in relative BLI signal in the hSSTR2⁺ teratomas exposed to $^{177}\text{Lu-DOTATATE}$ compared to the saline-treated group. This difference was significantly different at day 66 and day 80 post cell-injection (*p<0.05). **(C)** Quantification of the relative BLI signals of hNIS⁺ teratomas exposed to either $^{177}\text{Lu-DOTATATE}$ (n=4) or saline (n=4) showed no significant differences between both groups at all time points.

Successful differentiation of pluripotent stem cells towards cardiomyocyte-like cells with maintained reporter gene expression

As undifferentiated PSCs are not therapeutically relevant, gene-edited cells were differentiated towards CMs following the Gibco PSC CM differentiation kit. After 8 days, spontaneous beating could be observed in both gene-edited and WT ESCs, with an average beating frequency of 61 ± 26 bpm; 40 ± 18 bpm and 55 ± 34 bpm for hNIS⁺, hSSTR2⁺ and WT ESC-derived CMs, respectively (Figure 5A). After 15 days of differentiation, the pluripotency gene *SOX2* was downregulated in both hNIS⁺ (ΔCt of 1.7 ± 1.2 to -6.2 ± 1.1) and hSSTR2⁺ (ΔCt of 2.4 ± 3.4 to -2.2 ± 3.0) ESCs, as well as WT ESCs (ΔCt of 3.3 ± 2.1 to -4.1 ± 2.9) (Figure 5B). Differentiation towards CMs was demonstrated by the upregulation of early (*TBX5*) and late (cardiac myosin heavy chain (*cMHC*)) genetic markers of cardiomyogenesis. The *TBX5* transcript was upregulated after 15 days of cardiac differentiation in hNIS⁺ ESCs (ΔCt of -8.3 ± 2.2 to 2.5 ± 0.5), hSSTR2⁺ ESCs (ΔCt of -8.1 ± 3.0 to 2.8 ± 0.4) and WT ESCs (ΔCt of -7.9 ± 2.2 to -0.5 ± 3.3). This same upregulation was observed for *cMHC* after differentiation (hNIS⁺ ΔCt of -5.3 ± 2.8 to 6.9 ± 0.1 ; hSSTR2⁺ ΔCt of -4.9 ± 3.1 to 8.1 ± 1.5 ; WT ΔCt of -4.8 ± 2.7 to 3.4 ± 5.6) (Figure 5B). These findings were confirmed at the protein level by

immunofluorescence since all cell types tested positive for αSMA and CX-43 at day 15 of CM differentiation (Figure 5C).

After differentiation, cells were re-tested for functionality of the reporter genes. Both hSSTR2⁺ and hNIS⁺ ESC-derived CMs had significantly higher BLI signals after incubation with D-luciferin, in contrast to WT ESC-derived CMs (Figure 5D; $p<0.01$). After incubation with $^{99\text{m}}\text{TcO}_4$, both undifferentiated hNIS⁺ ESCs ($48.2\pm 1.6\%$) and hNIS⁺ ESC-derived CMs ($28.0\pm 8.7\%$) showed a tracer uptake that was significantly higher than WT ESCs ($0.9\pm 0.3\%$; $p<0.001$). Moreover, a significantly lower tracer uptake was present in the differentiated hNIS⁺ CMs compared to the undifferentiated hNIS⁺ ESCs ($p<0.001$) (Figure 5E). hSSTR2⁺ ESC-derived CMs, incubated with $^{68}\text{Ga-DOTATATE}$, showed a tracer uptake of $2.4\pm 0.4\%$, while undifferentiated hSSTR2⁺ ESCs had an uptake of $3.2\pm 0.4\%$. Only low tracer uptake was shown in WT ESCs ($0.5\pm 0.1\%$) (Figure 5F). Thus, a significantly higher tracer uptake was observed both in hSSTR2⁺ ESCs and hSSTR2⁺ ESC-derived CMs compared to WT ESCs ($p<0.001$), while no significant difference could be observed between the differentiated or undifferentiated state of hSSTR2⁺ cells ($p>0.05$).

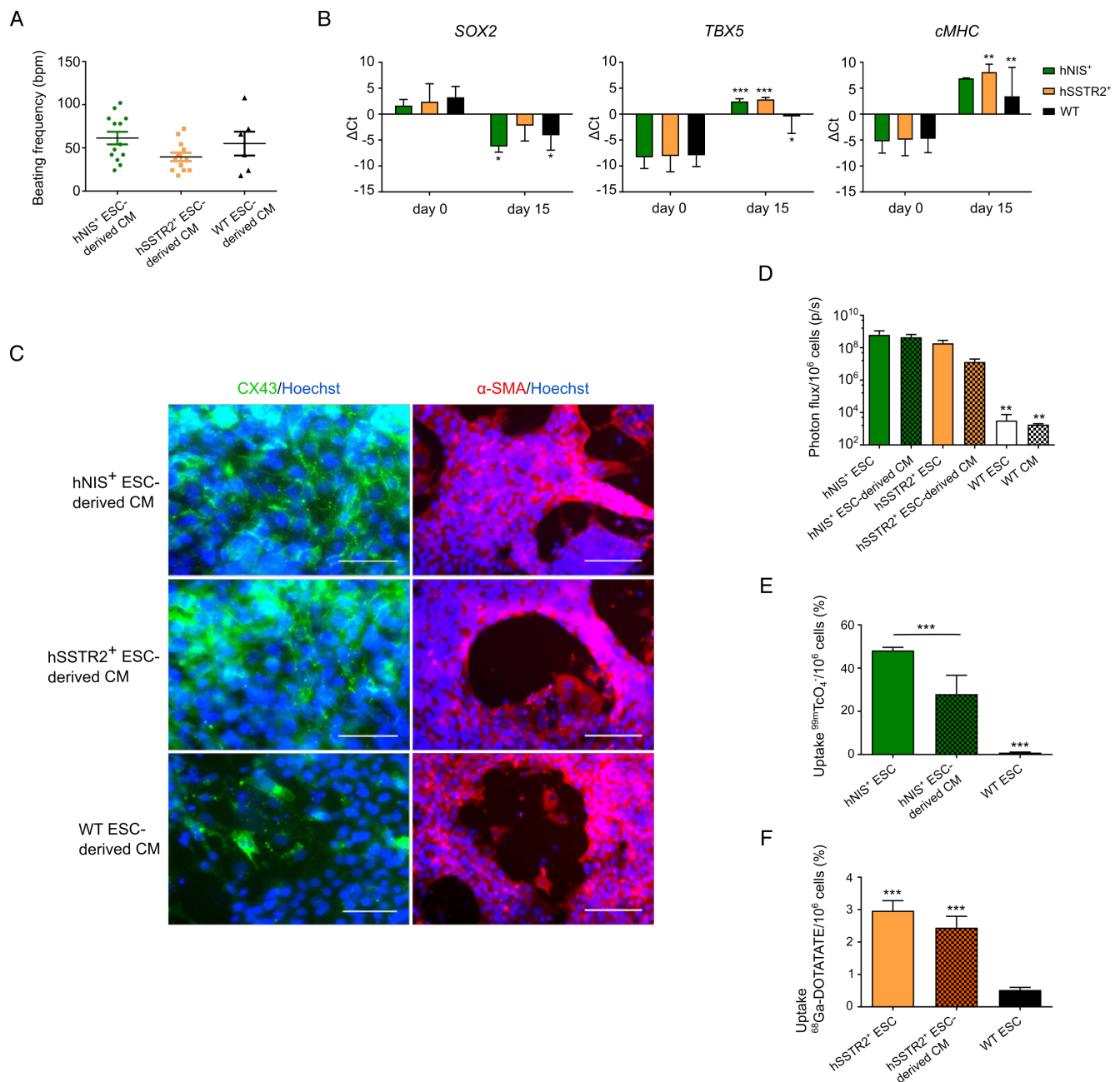


Figure 5. Differentiation of gene-edited PSCs towards CMs. (A) After 8 days of CM differentiation, spontaneous beating of the cells could be observed *in vitro*. No significant difference in beating frequency was seen between the different cell lines. (B) Differentiation towards CMs was also indicated by qRT-PCR, as there was a decrease in SOX2 expression at day 15 and upregulation of an early (TBX5) and late (cMHC) marker of cardiomyogenesis (*p<0.05; **p<0.01; ***p<0.001). (C) This was also confirmed at the protein level, as cells stained positive for CX-43 (green) and αSMA (red) at day 15 of differentiation (scale bar: 50 μm for CX-43 and 100 μm for αSMA). (D) Differentiation had no influence on reporter gene expression, as similar BLI signals were obtained from undifferentiated and differentiated ESCs (**p<0.01). (E) The uptake of ^{99m}TcO₄⁻ was significantly reduced after differentiation, although the uptake was still significantly higher than in WT ESCs (***p<0.001). (F) Similar uptake results were found for undifferentiated and differentiated hSSTR2⁺ ESCs after incubation with ⁶⁸Ga-DOTATATE. This was significantly higher than in WT ESCs (***p<0.001).

Intra-myocardial injection of hSSTR2⁺ embryonic stem cell-derived cardiomyocytes in an immune-deficient myocardial infarction mouse model

A MI was induced in Rag/γ2^{-/-} mice by permanent ligation of the LAD (n=4). Afterwards, one million hSSTR2⁺ ESC-derived CMs were injected at three sites of the MI border region. As a control, the

same set-up was used but animals received sham injections (n=4).

At day 10 post cell-injection, animals received an intravenous injection with ⁶⁸Ga-DOTATATE. In cell-injected animals, a clear tracer uptake in the heart region could be observed, while this was absent in the sham-injected animals (Figure 6A). Significantly higher mean SUVs were observed in the heart region of cell-injected (0.20±0.06) animals compared to sham-injected animals (0.04±0.01; p<0.01) (Figure 6B).

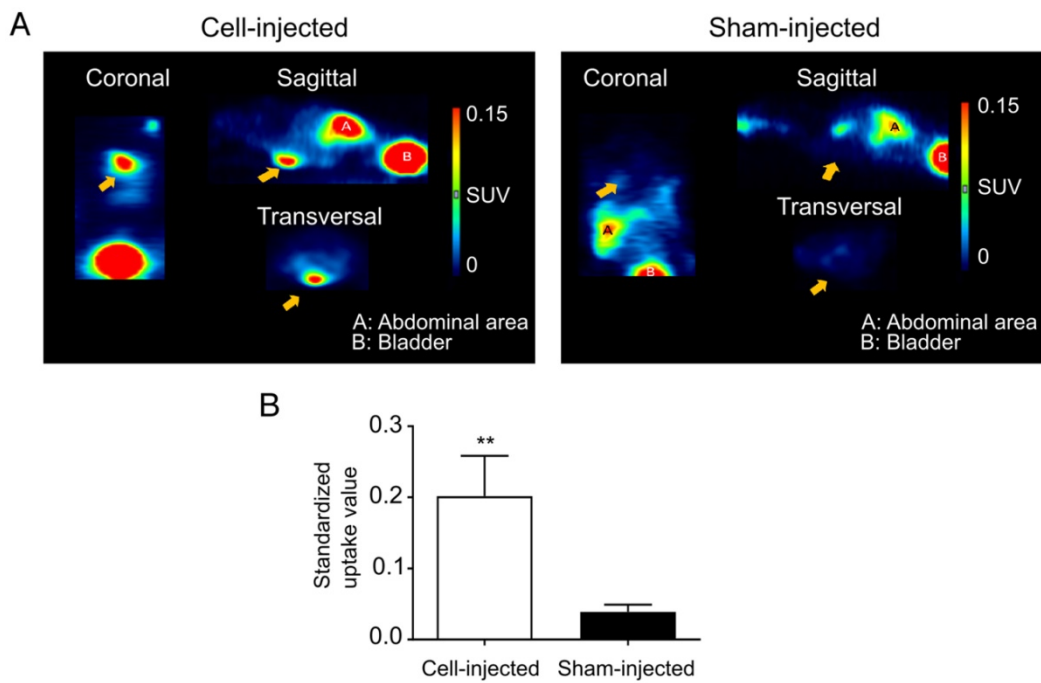


Figure 6. Visualization of hSSTR2⁺ ESC-derived CMs in the heart of mice with MI. (A) Representative images of MI mice injected either with hSSTR2⁺ CMs or sham. A clear focal uptake of ⁶⁸Ga-DOTATATE was shown in the heart region of the cell-injected animals, which was absent in the sham-injected animals. **(B)** Significantly higher tracer mean SUVs were observed in the heart region of cell-injected animals (n=3) compared to sham-injected animals (n=3) (**p<0.01).

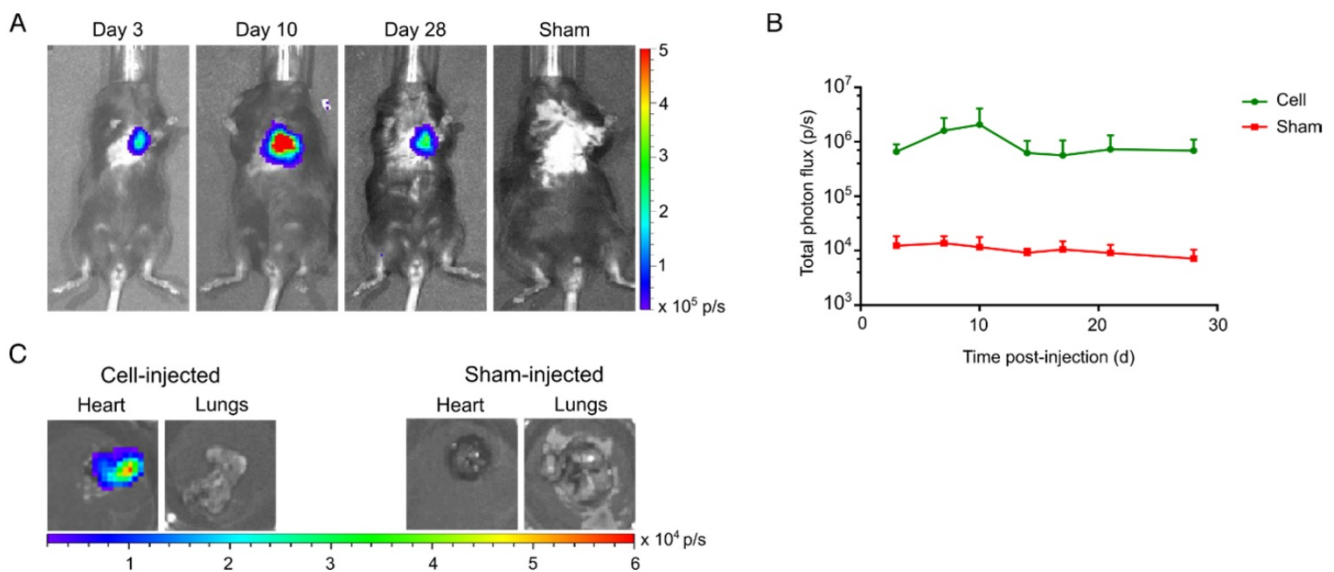


Figure 7. Long-term visualization of hSSTR2⁺ CMs in a murine MI model. (A) Representative BLI images of a cell- and sham-injected mouse with MI. **(B)** Quantification of BLI signals indicated an initial cell proliferation in the first 10 days after cell transplantation. Afterwards a reduction in BLI signal was observed until it became stable and reached similar values as 3 days post-injection. **(C)** *Ex vivo* BLI showed correct injection in the heart without spillage towards the lungs. No BLI signal was present in the sham-injected heart or lungs.

Clear BLI signals could be retrieved from the heart at day 3 post cell-injection ($6.6 \pm 1.2 \times 10^5$ p/s), while no BLI signals were observed in the sham-injected animals ($1.2 \pm 0.3 \times 10^4$ p/s) (Figure 7A). hSSTR2⁺ CMs showed an initial increase in BLI signal the first 10 days after injection ($2.1 \pm 1.0 \times 10^6$ p/s). Afterwards, a limited reduction in cell survival was observed. However, BLI signals at the end of the

experiment had similar values as three days post-injection (d3: $6.6 \pm 1.2 \times 10^5$ p/s; d28: $6.9 \pm 2.1 \times 10^5$ p/s) (Figure 7B). Upon sacrifice, an *ex vivo* BLI scan showed clear engraftment of the cells in the heart and absence of BLI signal from the lungs (Figure 7C).

MRI and calculation of the LVEF were performed to determine if the hSSTR2⁺ ESC-derived CMs had a therapeutic effect. Before permanent

ligation of the LAD, a baseline MRI scan showed a clear muscularized left ventricular wall (**Figure S2A**). Furthermore, both the cell- and sham-injected groups had similar LVEF before the procedure (cell: $73.9 \pm 2.3\%$; sham: $71.4 \pm 2.8\%$) (**Figure S2B**). After the induction of a MI, loss of CMs was seen together with an akinetic region of the heart (indicated by yellow arrow) (**Figure S2A**). This resulted in significantly reduced LVEF in both groups that continued to worsen over time (**Figure S2B**). Between the sham- and cell-injected groups, no difference was found in LVEF at week 1 (cell $53.3 \pm 10.4\%$; sham $55.7 \pm 13.7\%$), week 2 (cell $46.3 \pm 16.7\%$; sham $49.3 \pm 10.4\%$) and week 4 (cell $42.1 \pm 13.8\%$; sham $50.0 \pm 11.3\%$). On the four-chamber view, an indication of ventricular wall thickening was shown after one week in the cell-injected animals (indicated by green arrow). However, this did not persist over time (**Figure S2A**).

Discussion

The present work focuses on providing a safety-switch for PSC-derived cell therapy by using the hSSTr2 both as an imaging and suicide reporter gene. Here, we demonstrated that hSSTr2 allows long-term visualization of stem cell distribution and can detect potential uncontrolled cell proliferation. Furthermore, it allows intervention with a specific therapeutic radiopharmakon and therefore addresses an additional safety aspect towards translating PSC-derived therapies to the clinic.

Previously, incorporation of imaging reporter genes has mainly been performed by the use of retro- or lentiviral vectors that have the tendency to integrate in sites of active gene transcription. Therefore, there is a higher chance of insertional mutagenesis [22, 23]. Moreover, during differentiation or cell expansion, random reporter gene incorporation can result in genetic silencing [24]. Furthermore, heterogeneity is induced in the cell population as the reporter gene construct is integrated at different sites and each cell will carry different copy numbers of the reporter gene construct. The development of site-specific gene-editing by ZFNs avoids these disadvantages as a single copy of the reporter gene construct is integrated in a specific target site of the DNA, in our case the safe harbor locus AAVS1 [13, 14]. Our data is in accordance with literature since the integration in the AAVS1 locus did not impair pluripotency nor the differentiation capacity of the ESCs and allowed stable transgene expression over time both in pluripotent and differentiated cell state [13, 14, 19, 25]. Only in the $^{99m}\text{TcO}_4^-$ uptake experiment, a reduction in tracer uptake was observed in hNIS⁺ CMs. This can be caused by the use of a different medium to dissolve the tracer or, more

likely, by a decrease in the sodium gradient that drives hNIS-mediated $^{99m}\text{TcO}_4^-$ uptake in spontaneous contracting CMs. This last postulation is supported by the fact that there was no reduction of the *in vitro* BLI signal after differentiation, while Fluc and hNIS are linked to each other by a peptide 2A sequence. Furthermore, in a previous article by our group we demonstrated that tracer uptake was maintained after differentiation of hNIS⁺ ESCs towards hepatocytes [19].

At present, stem cell therapy is struggling in the clinic to reach the beneficial effects observed in pre-clinical research. One of the issues is the inability to monitor stem cell fate in a clinical setting, as tissue biopsies are limited. Therefore, molecular and cellular imaging can provide an essential tool to visualize the bio-distribution and viability of the cells noninvasively over time [9, 26]. To allow clinical translation, we have used two human radionuclide reporter genes, hNIS and hSSTr2, which avoid immunogenicity and allow cell tracking with clinical radionuclide imaging devices.

In this study, we confirmed that PET allows long-term PSC tracking after site-specific gene-editing [19]. hNIS is a relatively well-established radionuclide reporter gene that has been shown to track cells both in rodents [20, 27] and in larger animals [15, 17]. The feasibility to use hNIS for monitoring murine teratoma formation, after stable murine ESC transfection, has also been demonstrated by Lehner et al. [28]. In contrast, hSSTr2 has not been frequently used for cell tracking.

The use of imaging reporter genes allowed us to visualize the neoplastic teratoma growth, noninvasively. As a limitation, the increase in total lesion uptake of ^{68}Ga -DOTATATE and ^{124}I in both hSSTr2⁺ and hNIS⁺ teratomas respectively, was limited. Therefore, it might be advisable to combine the imaging methods with analysis of serum biomarkers indicative for teratoma formation as determined by Riegler et al. [29]. However, it should be noted that these biomarkers are a consequence of PSC differentiation and do not detect PSCs, the neoplastic part of the teratoma. This was highlighted further by the fact that they were unable to detect one out of the eight teratomas. Furthermore, they are highly dependent on the differentiated progeny and a broad multicenter study should be performed to test the consistency of these biomarkers in teratomas derived from different cell origins. Within our study, these biomarkers could not be tested as insufficient blood could be retrieved from the mice.

Although PSCs have an enormous potential for the regenerative medicine field, the risk of neoplastic lesion formation still exists because of remaining PSCs

in the cell mixture after differentiation or the potential transdifferentiation towards their PSC state. Therefore, we assessed hSSTR2 not only as an imaging reporter gene but also as a suicide gene. SSTR2 is overexpressed on NETs, and peptide receptor radionuclide therapy with ^{177}Lu -DOTATATE has demonstrated to have a significantly higher response rate than high-dose octreotide. Furthermore, the recently published phase III NETTER-1 trial showed that patients with a SSTR2⁺ midgut NET had an increased progression-free survival after ^{177}Lu -DOTATATE treatment [18]. In this study, we confirmed specific cell killing of hSSTR2⁺ cells after ^{177}Lu -DOTATATE exposure. After *in vitro* exposure of hSSTR2⁺ cells to ^{177}Lu -DOTATATE, a significant decrease in cell survival was seen both by BLI and Hoechst staining. However, different kinetics could be observed between these two methods. This suggests that different cell plating densities at the start of the experiment cause a difference in cell survival kinetics. In addition, we are the first to demonstrate that *in vivo* ^{177}Lu -DOTATATE exposure was associated with decreased total ^{68}Ga -DOTATATE uptake in hSSTR2⁺ teratomas and a reduction in teratoma size compared to saline-treated hSSTR2⁺ teratomas. As a confirmation of the cytotoxic effect of ^{177}Lu -DOTATATE on hSSTR2⁺ and not hNIS⁺ ESCs, *in vivo* BLI was performed in addition to PET imaging. Indeed, the BLI signal decreased in hSSTR2⁺ teratomas after ^{177}Lu -DOTATATE exposure, which was not the case for the hNIS⁺ cells. It can be noted that different baseline BLI signals were present before therapy in hSSTR2⁺ and hNIS⁺ teratomas, which can be explained by the fact that different cell lines generate different teratoma morphologies [19]. In addition, hSSTR2-expressing teratomas might have a decreased proliferation rate as it is known that receptor activation inhibits cell growth [30, 31]. However, when we look to hSSTR2⁺ or hNIS⁺ teratomas separately, comparable BLI signals could be observed the day before administration of ^{177}Lu -DOTATATE or saline, allowing us to make the assessment on the effect of ^{177}Lu -DOTATATE on teratoma growth. Moreover, our imaging-based approach gives the possibility to monitor each individual teratoma longitudinally. Therefore, our results were expressed as relative lesion uptake or relative BLI signal to account for the unavoidable differences in baseline teratoma size. Despite ^{177}Lu -DOTATATE treatment, still a small teratoma lesion could be retrieved upon sacrifice of the animals. Therefore, it might be advisable to perform repeated rounds of ^{177}Lu -DOTATATE administration, as it has been shown to enhance therapeutic outcome and is standardly performed in a clinical setting [18, 32].

In the literature, the most widely used combined imaging and suicide gene is the herpes simplex virus type 1 thymidine kinase (HSV-tk) reporter gene. PSC overexpressing HSV-tk have been generated and noninvasively monitored by PET [33]. In addition, several groups showed that selective killing of HSV-tk-overexpressing ESCs was feasible after continuous exposure to ganciclovir (GCV). Unfortunately, they did not combine this with noninvasive cell monitoring [33-36]. In the majority of the studies, no complete removal of the teratomas could be obtained, as was the case for our ^{177}Lu -DOTATATE-based approach. In contrast, the suicide gene HSV-tk has already been successful in different clinical trials as a safety-switch upon development of graft-versus-host disease (GVHD) [37-41]. Administration of GCV resulted in complete removal of the infused genetically engineered lymphocytes and the associated GVHD [37-41]. This discrepancy in complete graft removal can be explained by the fact that teratomas consist of a mixture of differentiated and undifferentiated cells. Since terminally differentiated cells do not divide anymore, they become resistant to GCV treatment [41, 42]. Similarly, these non-dividing cells might be more resistant to radiotherapy, but after repeated cycles of ^{177}Lu -DOTATATE exposure the cumulative dose might be high enough to induce cell death in terminally differentiated cells. The major advantage of the GCV-HSV-tk system is the absence of any adverse events, even after continuous exposure, since the viral thymidine kinase (TK) has a 1000-fold higher efficiency in converting GCV towards its cytotoxic metabolite than mammalian mitochondrial TK [38-41, 43]. This is not feasible with radionuclide therapy since the radionuclide as such is the cytotoxic part and not a metabolite of the administered substrate. Furthermore, SSTR2 is endogenously expressed in certain tissues, leading to specific accumulation of ^{177}Lu -DOTATATE in these organs. The phase III NETTER-1 trial demonstrated mainly limited grade 1 or 2 adverse events (abdominal pain, fatigue, thrombocytopenia, etc.). Only in 1%, 2%, and 9% of patients receiving ^{177}Lu -DOTATATE, were grade 3 or 4 neutropenia, thrombocytopenia or lymphopenia observed, respectively [18]. Despite the fact that the safety profile of the GCV-HSV-tk system is superior compared to our proposed ^{177}Lu -DOTATATE-hSSTR2 system, we do believe that our approach holds merit as it has been demonstrated that specific immunization towards the viral HSV-tk can occur [37, 39], while our system is of human origin. Furthermore, it does not prohibit the use of antiviral treatment [44]. Lastly, as HSV-TK is a cytoplasmic protein, an additional surface marker needs to be

incorporated into the reporter gene construct to allow selection of the transduced cells [37, 39-41]. In contrast, our hSSTR2 is a membrane receptor that can immediately be used to isolate the hSSTR2⁺ cell population.

hNIS was not used as suicide gene since no stable radionuclide incorporation could be achieved due to the lack of iodide organification, thus resulting in substantial tracer elution from the cells. Therefore, we believe that hSSTR2 is a better alternative as it allows long-term radiopharmaceutical retention. However, some groups have demonstrated the feasibility of using ¹³¹I or ¹⁸⁸Rh for killing hNIS-overexpressing cells [45-49]. While they also observed a similar efflux of the radiopharmaceutical both *in vitro* and *in vivo*, an *in vivo* retention time of less than one day was apparently long enough to exert the toxic effects if repeated administration was performed [46-48].

As undifferentiated PSCs are not therapeutically relevant, we have differentiated them towards CMs. As previously described, this resulted in spontaneously contracting CMs expressing CX-43 [50]. Upon transplantation in a MI mouse model, long-term cell survival could be achieved. Like previously demonstrated by Laflamme et al., proliferation of the transplanted CMs occurred the first days post-injection, indicated by an increase in BLI signal from day 3 to day 10 [51]. In contrast to the study by Laflamme et al., this increased proliferation did not persist until week 4 and after 10 days a reduction in BLI signal was shown, indicating that not all cells had a permanent and successful engraftment. This *in vivo* cell behavior might be explained by the fact that we injected the cells in matrigel, full of growth factors, which might boost cell proliferation in the initial days. The reduction afterwards might be mediated by the growing infarct area over time induced by the permanent ligation of the LAD. At the end of the experiment (day 28), similar BLI signals were demonstrated compared to day 3 post-injection, indicating a high engraftment rate and long-term survival of these hSSTR2⁺ ESC-derived CMs.

Despite long-term cell survival, no therapeutic effect was seen. The absence of a therapeutic effect might be explained by the high heart rate of rodents compared to the human heart and our human ESC-derived CMs. Other groups already showed that arrhythmias by human PSC-derived CMs only appeared in larger animal models with MI and were not detected in rodents with MI [2-4]. Unfortunately, we were only able to visualize cell survival and not electrical coupling of our injected CMs. This would provide us with information on the functionality of the cells *in vivo*. Another reason to evaluate

PSC-derived therapy in larger animals is the ability to do echo-guided injections, thereby allowing controlled cell injections in the close proximity of the infarct. With our radionuclide imaging reporter genes, we would then still be able to track the cells via PET. To achieve therapeutic efficacy, a milder MI model, namely ischemia/reperfusion, might be more beneficial as a chronic ligation is potentially too severe to repair with cell therapy. By the use of an ischemia/reperfusion model in rats, successful PSC-derived CM therapy has been achieved by Laflamme et al [1].

Conclusion

In this study, we have generated isogenic ESCs via ZFN-based gene-editing, expressing human radionuclide imaging reporter genes that have the potential for regulatory approval and can be used for cell monitoring in various cell therapy applications via clinical radionuclide imaging devices. As PSC-derived cell therapy does not yield 100% purity, the risk for neoplastic teratoma formation is still present. We are the first to demonstrate that hSSTR2-based radionuclide therapy can be used as a safety-switch in case of unwanted teratoma development. The safe reporter gene incorporation and double role of hSSTR2 as a radionuclide imaging and suicide gene further increases the potential of stem cell reporter gene-based imaging to become clinically applied.

Abbreviations

AAVS1: adeno-associated virus integration site 1; BLI: bioluminescence imaging; CM: cardiomyocyte; cMHC: cardiac myosin heavy chain; ESC: embryonic stem cell; Fluc: firefly luciferase; GCV: ganciclovir; GVHD: graft-versus-host disease; hNIS: human sodium iodide symporter; hSSTR2: human somatostatin receptor type 2; HSV-tk: herpes simplex virus type 1 thymidine kinase; IE: independent experiment; LAD: left anterior descending coronary artery; LVEF: left ventricular ejection fraction; MI: myocardial infarction; MRI: magnetic resonance imaging; NET: neuroendocrine tumor; PET: positron emission tomography; PSC: pluripotent stem cell; qRT-PCR: quantitative real-time PCR; SUV: standardized uptake value; TK: thymidine kinase; TR: technical replicate; VOI: volume of interest; WT: wild-type; ZFN: zinc finger nuclease; α SMA: α -smooth muscle actin.

Supplementary Material

Supplementary figures.

<http://www.thno.org/v08p2799s1.pdf>

Competing interests

Katrien Neyrinck works as an aspirant for the FWO, while both Natacha Breuls and Bryan Holvoet work under an SB-grant of the FWO. Christophe M. Deroose is a consultant for Advanced Accelerator Applications (AAA) and Novartis, who hold rights to commercialize ¹⁷⁷Lu-DOTATATE. He is also a consultant for Sirtex, Bayer, Ipsen and Terumo. He received travel grants from GE Healthcare. No other potential conflict of interest relevant to this article was reported.

References

1. Laflamme MA, Chen KY, Naumova AV, Muskheli V, Fugate JA, Dupras SK, et al. Cardiomyocytes derived from human embryonic stem cells in pro-survival factors enhance function of infarcted rat hearts. *Nat Biotechnol.* 2007; 25: 1015-24.
2. Shiba Y, Fernandes S, Zhu WZ, Filice D, Muskheli V, Kim J, et al. Human ES-cell-derived cardiomyocytes electrically couple and suppress arrhythmias in injured hearts. *Nature.* 2012; 489: 322-5.
3. Shiba Y, Gombibuchi T, Seto T, Wada Y, Ichimura H, Tanaka Y, et al. Allogeneic transplantation of iPSC cell-derived cardiomyocytes regenerates primate hearts. *Nature.* 2016; 538: 388-91.
4. Chong JJ, Yang X, Don CW, Minami E, Liu YW, Weyers JJ, et al. Human embryonic-stem-cell-derived cardiomyocytes regenerate non-human primate hearts. *Nature.* 2014; 510: 273-7.
5. Laflamme MA, Murry CE. Heart regeneration. *Nature.* 2011; 473: 326-35.
6. Lee AS, Tang C, Rao MS, Weissman IL, Wu JC. Tumorigenicity as a clinical hurdle for pluripotent stem cell therapies. *Nat Med.* 2013; 19: 998-1004.
7. Menasche P, Vanneaux V, Hagege A, Bel A, Cholley B, Cacciapuoti I, et al. Human embryonic stem cell-derived cardiac progenitors for severe heart failure treatment: first clinical case report. *Eur Heart J.* 2015; 36: 2011-7.
8. Holvoet B, De Waele L, Quattrocchi M, Gheysens O, Sampaolesi M, Verfaillie CM, et al. Increased Understanding of Stem Cell Behavior in Neurodegenerative and Neuromuscular Disorders by Use of Noninvasive Cell Imaging. *Stem Cells Int.* 2016; 2016: 6235687.
9. Himmelreich U, Dresselaers T. Cell labeling and tracking for experimental models using magnetic resonance imaging. *Methods.* 2009; 48: 112-24.
10. Hacein-Bey-Abina S, Hauer J, Lim A, Picard C, Wang GP, Berry CC, et al. Efficacy of gene therapy for X-linked severe combined immunodeficiency. *N Engl J Med.* 2010; 363: 355-64.
11. Sakuma T, Barry MA, Ikeda Y. Lentiviral vectors: basic to translational. *Biochem J.* 2012; 443: 603-18.
12. Collin J, Lako M. Concise review: putting a finger on stem cell biology: zinc finger nuclease-driven targeted genetic editing in human pluripotent stem cells. *Stem Cells.* 2011; 29: 1021-33.
13. Hockemeyer D, Soldner F, Beard C, Gao Q, Mitalipova M, DeKaveler RC, et al. Efficient targeting of expressed and silent genes in human ESCs and iPSCs using zinc-finger nucleases. *Nat Biotechnol.* 2009; 27: 851-7.
14. DeKaveler RC, Choi VM, Moehle EA, Paschon DE, Hockemeyer D, Meijnsing SH, et al. Functional genomics, proteomics, and regulatory DNA analysis in isogenic settings using zinc finger nuclease-driven transgenesis into a safe harbor locus in the human genome. *Genome Res.* 2010; 20: 1133-42.
15. Lee AR, Woo SK, Kang SK, Lee SY, Lee MY, Park NW, et al. Adenovirus-mediated expression of human sodium-iodide symporter gene permits in vivo tracking of adipose tissue-derived stem cells in a canine myocardial infarction model. *Nucl Med Biol.* 2015; 42: 621-9.
16. Shi S, Zhang M, Guo R, Miao Y, Zhang X, Li B. Molecular imaging to monitor repair of myocardial infarction using genetically engineered bone marrow-derived mesenchymal stem cells. *Curr Gene Ther.* 2015; 15: 460-71.
17. Templin C, Zweigerdt R, Schwanke K, Olmer R, Ghadri JR, Emmert MY, et al. Transplantation and tracking of human-induced pluripotent stem cells in a pig model of myocardial infarction: assessment of cell survival, engraftment, and distribution by hybrid single photon emission computed tomography/computed tomography of sodium iodide symporter transgene expression. *Circulation.* 2012; 126: 430-9.
18. Strosberg J, El-Haddad G, Wolin E, Hendifar A, Yao J, Chasen B, et al. Phase 3 Trial of ¹⁷⁷Lu-Dotatate for Midgut Neuroendocrine Tumors. *N Engl J Med.* 2017; 376: 125-35.
19. Wolfs E, Holvoet B, Ordovas L, Breuls N, Helsen N, Schonberger M, et al. Molecular imaging of human embryonic stem cells stably expressing human PET reporter genes after zinc finger nucleases-mediated genome editing. *J Nucl Med.* 2017.
20. Holvoet B, Quattrocchi M, Belderbos S, Pollaris L, Wolfs E, Gheysens O, et al. Sodium Iodide Symporter PET and BLI Noninvasively Reveal Mesoangioblast Survival in Dystrophic Mice. *Stem Cell Reports.* 2015; 5: 1183-95.
21. Jacobs G, Oosterlinck W, Dresselaers T, Geenens R, Kerselaers S, Himmelreich U, et al. Enhanced beta-adrenergic cardiac reserve in Trpm4(-)/(-) mice with ischaemic heart failure. *Cardiovasc Res.* 2015; 105: 330-9.
22. Hacein-Bey-Abina S, Von Kalle C, Schmidt M, McCormack MP, Wulffraat N, Leboulch P, et al. LMO2-associated clonal T cell proliferation in two patients after gene therapy for SCID-X1. *Science.* 2003; 302: 415-9.
23. Hacein-Bey-Abina S, Garrigue A, Wang GP, Soulier J, Lim A, Morillon E, et al. Insertional oncogenesis in 4 patients after retrovirus-mediated gene therapy of SCID-X1. *J Clin Invest.* 2008; 118: 3132-42.
24. Ellis J. Silencing and variegation of gammaretrovirus and lentivirus vectors. *Human Gene Therapy.* 2005; 16: 1241-6.
25. Wang Y, Zhang WY, Hu S, Lan F, Lee AS, Huber B, et al. Genome editing of human embryonic stem cells and induced pluripotent stem cells with zinc finger nucleases for cellular imaging. *Circ Res.* 2012; 111: 1494-503.
26. Wolfs E, Verfaillie CM, Van Laere K, Deroose CM. Radiolabeling strategies for radionuclide imaging of stem cells. *Stem Cell Rev.* 2015; 11: 254-74.
27. Lee HW, Yoon SY, Singh TD, Choi YJ, Lee HJ, Park JY, et al. Tracking of dendritic cell migration into lymph nodes using molecular imaging with sodium iodide symporter and enhanced firefly luciferase genes. *Sci Rep.* 2015; 5: 9865.
28. Lehner S, Lang C, Kaissis G, Todica A, Zacherl MJ, Boening G, et al. (124)I-PET Assessment of Human Sodium Iodide Symporter Reporter Gene Activity for Highly Sensitive In Vivo Monitoring of Teratoma Formation in Mice. *Mol Imaging Biol.* 2015; 17: 874-83.
29. Riegler J, Ebert A, Qin X, Shen Q, Wang M, Ameen M, et al. Comparison of Magnetic Resonance Imaging and Serum Biomarkers for Detection of Human Pluripotent Stem Cell-Derived Teratomas. *Stem Cell Reports.* 2016; 6: 176-87.
30. Kvols LK, Moertel CG, Oconnell MJ, Schutt AJ, Rubin J, Hahn RG. Treatment of the Malignant Carcinoid-Syndrome - Evaluation of a Long-Acting Somatostatin Analog. *New Engl J Med.* 1986; 315: 663-6.
31. Rinke A, Muller HH, Schade-Brittinger C, Klose KJ, Barth P, Wied M, et al. Placebo-Controlled, Double-Blind, Prospective, Randomized Study on the Effect of Octreotide LAR in the Control of Tumor Growth in Patients With Metastatic Neuroendocrine Midgut Tumors: A Report From the PROMID Study Group. *J Clin Oncol.* 2009; 27: 4656-63.
32. Schmitt A, Bernhardt P, Nilsson O, Ahlman H, Kolby L, Maecke HR, et al. Radiation therapy of small cell lung cancer with ¹⁷⁷Lu-DOTA-Tyr3-octreotate in an animal model. *J Nucl Med.* 2004; 45: 1542-8.
33. Cao F, Lin S, Xie X, Ray P, Patel M, Zhang X, et al. In vivo visualization of embryonic stem cell survival, proliferation, and migration after cardiac delivery. *Circulation.* 2006; 113: 1005-14.
34. Schuldiner M, Itskovitz-Eldor J, Benvenisty N. Selective ablation of human embryonic stem cells expressing a "suicide" gene. *Stem Cells.* 2003; 21: 257-65.
35. Cao F, Drukker M, Lin S, Sheikh AY, Xie X, Li Z, et al. Molecular imaging of embryonic stem cell misbehavior and suicide gene ablation. *Cloning Stem Cells.* 2007; 9: 107-17.
36. Leten C, Roobrouck VD, Struys T, Burns TC, Dresselaers T, Vande Velde G, et al. Controlling and monitoring stem cell safety in vivo in an experimental rodent model. *Stem Cells.* 2014; 32: 2833-44.
37. Ciceri F, Bonini C, Markt S, Zappone E, Servida P, Bernardi M, et al. Antitumor effects of HSV-TK-engineered donor lymphocytes after allogeneic stem-cell transplantation. *Blood.* 2007; 109: 4698-707.
38. Tiberghien P, Ferrand C, Lioure B, Milpied N, Angonin R, Deconinck E, et al. Administration of herpes simplex-thymidine kinase-expressing donor T cells with a T-cell-depleted allogeneic marrow graft. *Blood.* 2001; 97: 63-72.
39. Bonini C, Ferrari G, Verzeletti S, Servida P, Zappone E, Ruggieri L, et al. HSV-TK gene transfer into donor lymphocytes for control of allogeneic graft-versus-leukemia. *Science.* 1997; 276: 1719-24.
40. Ciceri F, Bonini C, Stanghellini MT, Bondanza A, Traversari C, Salomoni M, et al. Infusion of suicide-gene-engineered donor lymphocytes after family haploidentical haemopoietic stem-cell transplantation for leukaemia (the TK007 trial): a non-randomised phase I-II study. *Lancet Oncol.* 2009; 10: 489-500.
41. Borchers S, Provasi E, Silvani A, Radrizzani M, Benati C, Dammann E, et al. Genetically modified donor leukocyte transfusion and graft-versus-leukemia effect after allogeneic stem cell transplantation. *Human Gene Therapy.* 2011; 22: 829-41.
42. Cieri N, Mastaglio S, Oliveira G, Casucci M, Bondanza A, Bonini C. Adoptive immunotherapy with genetically modified lymphocytes in allogeneic stem cell transplantation. *Immunol Rev.* 2014; 257: 165-80.
43. Portsmouth D, Hlavaty J, Renner M. Suicide genes for cancer therapy. *Mol Aspects Med.* 2007; 28: 4-41.
44. Gambhir SS, Bauer E, Black ME, Liang Q, Kokoris MS, Barrio JR, et al. A mutant herpes simplex virus type 1 thymidine kinase reporter gene shows improved sensitivity for imaging reporter gene expression with positron emission tomography. *Proc Natl Acad Sci U S A.* 2000; 97: 2785-90.
45. Knoop K, Schwenk N, Schmohl K, Muller A, Zach C, Cyran C, et al. Mesenchymal stem cell-mediated, tumor stroma-targeted radiiodine therapy of metastatic colon cancer using the sodium iodide symporter as theranostic gene. *J Nucl Med.* 2015; 56: 600-6.
46. Zhang M, Shi S, Guo R, Miao Y, Li B. Use of rhenium-188 for in vivo imaging and treatment of human cervical cancer cells transfected with lentivirus expressing sodium iodide symporter. *Oncol Rep.* 2016; 36: 2289-97.
47. Muller AM, Schmohl KA, Knoop K, Schug C, Urnauer S, Hagenhoff A, et al. Hypoxia-targeted ¹³¹I therapy of hepatocellular cancer after systemic

- mesenchymal stem cell-mediated sodium iodide symporter gene delivery. *Oncotarget*. 2016; 7: 54795-810.
48. Guo R, Zhang M, Xi Y, Ma Y, Liang S, Shi S, et al. Theranostic studies of human sodium iodide symporter imaging and therapy using ¹⁸⁸Re: a human glioma study in mice. *PLoS One*. 2014; 9: e102011.
49. Tang J, Wang X, Xu Y, Shi Y, Liu Z, Yang Y. Sodium-iodine symporter gene expression controlled by the EGR-1 promoter: biodistribution, imaging and in vitro radionuclide therapy with Na(¹³¹)I. *Technol Cancer Res Treat*. 2015; 14: 61-9.
50. Dell'Era P, Benzoni P, Crescini E, Valle M, Xia E, Consiglio A, et al. Cardiac disease modeling using induced pluripotent stem cell-derived human cardiomyocytes. *World J Stem Cells*. 2015; 7: 329-42.
51. Laflamme MA, Gold J, Xu C, Hassanipour M, Rosler E, Police S, et al. Formation of human myocardium in the rat heart from human embryonic stem cells. *Am J Pathol*. 2005; 167: 663-71.